

## Convergence-aligned foreland magmatism in the Arabia–Anatolia Collision: geochronological evidence from the Karacadağ Volcanic Complex, south-east Turkey

Taner EKİCİ<sup>1\*</sup>, Colin G. MACPHERSON<sup>2</sup>

<sup>1</sup>Department of Geological Engineering, Faculty of Engineering, Sivas Cumhuriyet University, Sivas, Turkey

<sup>2</sup>Department of Earth Sciences, University of Durham, Durham, UK

Received: 19.02.2019 • Accepted/Published Online: 24.06.2019 • Final Version: 04.09.2019

**Abstract:** New <sup>40</sup>Ar/<sup>39</sup>Ar ages are presented for volcanic rocks from the Karacadağ Volcanic Complex (KVC) in SE Anatolia. These extend the oldest age recognised for the KVC for lavas from the Siverek Phase plateau basalt back to at least 17 Ma. Our data agree with prior studies that the second, Karacadağ Phase of igneous activity began at about 4.5 Ma with a peak between 2 and 1 Ma, but in contrast to previous work we find that this included volcanism on the Mt. Karacadağ ridge from the earliest part of this phase. Construction of the Mt. Karacadağ ridge coincided with development of the prominent east–west striking Abd El Aziz and Sinjar compressional antiforms, which lie approximately 100 km to the south. These provide complementary evidence for the orientation of compressional deformation across a broad zone of the leading edge of the Arabian Plate as it collided with Anatolia between 4 and 1 Ma. The new data also indicate that the compression-aligned deformation of the foreland magmatism may have permitted tapping of melts from greater depth in the probably asthenospheric mantle than occurred prior to 4 Ma. However, magmas from throughout the history of the KVC contain some components derived from the lithospheric mantle.

**Key words:** Karacadağ Volcanic Complex, magmatism collision, compression, <sup>40</sup>Ar/<sup>39</sup>Ar

### 1. Introduction

Stress fields in orogenic zones can influence the distribution of resources and also control the long-term evolution of structures in collision zones (Brew et al., 1999; Allen et al., 2004). Magmatic rocks can provide a valuable tool to understand the development of these stress fields, which will focus magma transport and therefore control preferred orientations of igneous bodies or their constituent minerals. Radiometric dating provides a means to place absolute constraints upon when such stress was present.

We present new geochronological data for Neogene to Quaternary lavas from the Karacadağ Volcanic Complex (KVC) in the foreland of the Arabia–Anatolia collision zone (Figures 1–3). This complex has been subject to several recent geologic and petrologic studies (Lustrino et al., 2010, 2012; Ekici et al., 2012, 2014; Koçbulut et al., 2013; Keskin et al., 2012a, 2012b; Seyitoğlu et al., 2017) that have substantially augmented our prior understanding of both magma sources and magmatic plumbing (Pearce et al., 1990). We present new <sup>40</sup>Ar–<sup>39</sup>Ar age data to show that the Plio–Pleistocene magmatic history of the northern Arabian Plate is intimately linked to tectonic and neighbouring structural features of the upper crust,

providing an additional constraint on the development of these structures. The data also provide enhanced context for interpreting the recently expanded geochemical dataset to explore how local collision tectonic forces may have influenced the generation and transport of magma.

### 2. Geological setting and the Karacadağ Volcanic Complex

#### 2.1. Geological setting

The KVC in south-east Turkey lies immediately south of the Arabian–Anatolian collision zone (Figures 1 and 2). This collision is the result of northward motion of the Arabian Plate with respect to Eurasia and the Anatolian Plate (Allen et al., 2004).

Rifting caused lithosphere subsidence of the northern Arabian in the Carboniferous, affecting a NE–SW belt that formed the deposits of the present day Palmyride Mountain Belt to the Sinjar region of NW Iraq (Brew et al., 1999). During the Late Cretaceous the development of the Euphrates fault system disrupted this continuous belt by inverting the Mesozoic deposits, ultimately resulting in the development of the Palmyride Fold Belt (Searle, 1994). Palaeocene subduction of the Neo-Tethyan oceanic

\* Correspondence: tanere7@gmail.com

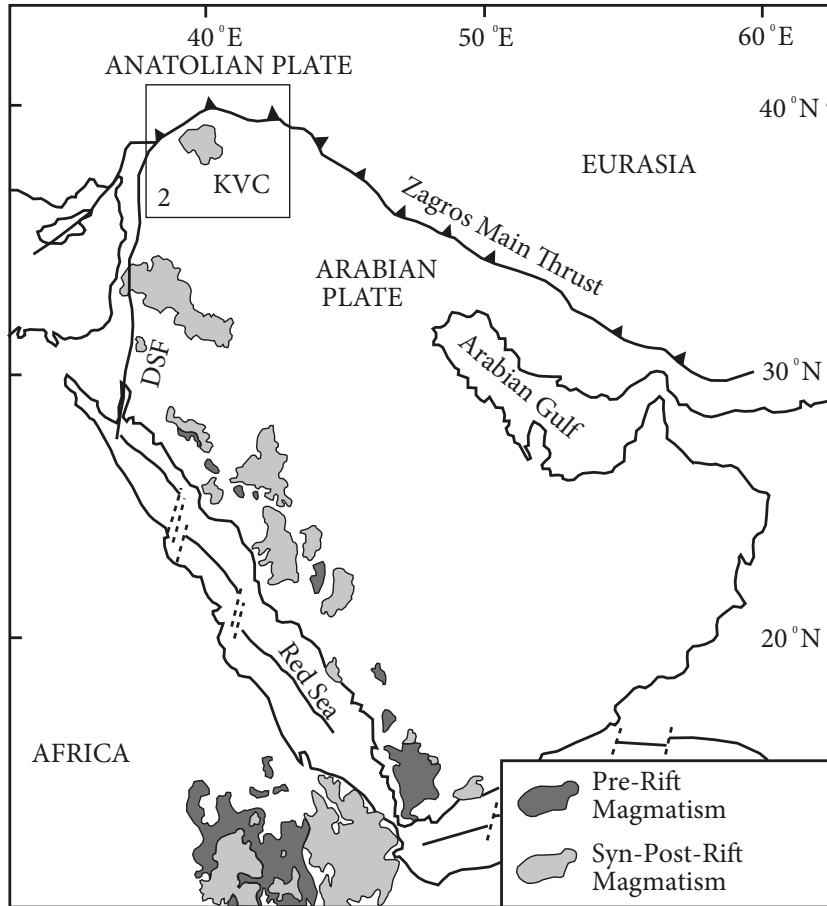


**Figure 1.** Major tectonic boundaries and distribution of Cenozoic magmatism on the Arabian Plate. “Pre-Rift” and “Post-Rift” refer to the opening of the Red Sea. KVC: Karacadağ Volcanic Complex; DSF: Dead Sea Fault. Box shows location of Figure 2. Maps modified from Ilani et al. (2001), Bosworth et al. (2005), Gürsoy et al. (2009), and Krienitz et al. (2009).

lithosphere beneath Anatolia led to the formation of the Bitlis Suture due to collision of Arabia with Anatolia (Figure 2). Continued convergence between Arabia and Eurasia led to westward extrusion of Anatolia along the Northern and Eastern Anatolian faults during the Late Miocene (Robertson, 2000; Şengör et al., 2008).

Of note for this study is the subsequent deposition of mainly marly limestones that occurred in the E–W trending Sinjar–Abd el Aziz area. Similar reactivation of normal faults associated with preceding extensional systems has occurred throughout the Cenozoic in this area but was most marked in the Plio–Pleistocene uplift of the prominent E–W Sinjar and Abd el Aziz inversion structures, which are thought to present about 1% lithospheric shortening (Brew et al., 1999). The KVC formed on the leading edge of the Arabian Plate during its collision with Anatolia.

## 2.2. The Karacadağ Volcanic Complex (KVC)

The KVC has produced three phases of volcanism since the Middle Miocene. The first of these plateau basalts is referred to as the Siverek Phase. The second phase is the Karacadağ Phase, which produced the most prominent KVC feature, Mt. Karacadağ. This is a north–south striking shield volcano of approximately 25 km in length (Figure 3) that was constructed during the Late Miocene to Pleistocene as a series of vents and cones erupting alkali basaltic and basanitic lavas above a presumed fissure system (Ercan et al., 1990; Pearce et al., 1990; Adiyaman and Chorowicz, 2002; Keskin, 2003, 2012a, 2012b; Şen et al., 2004; Brigland et al., 2007; Demir et al., 2007; Lustrino et al., 2010; Ekici et al., 2014). The third and final phase, called the Ovabağ Phase, comprises low volumes of alkali basalt and basanite that were erupted around the village of Ovabağ, to the east of Mt. Karacadağ (Figure 3).

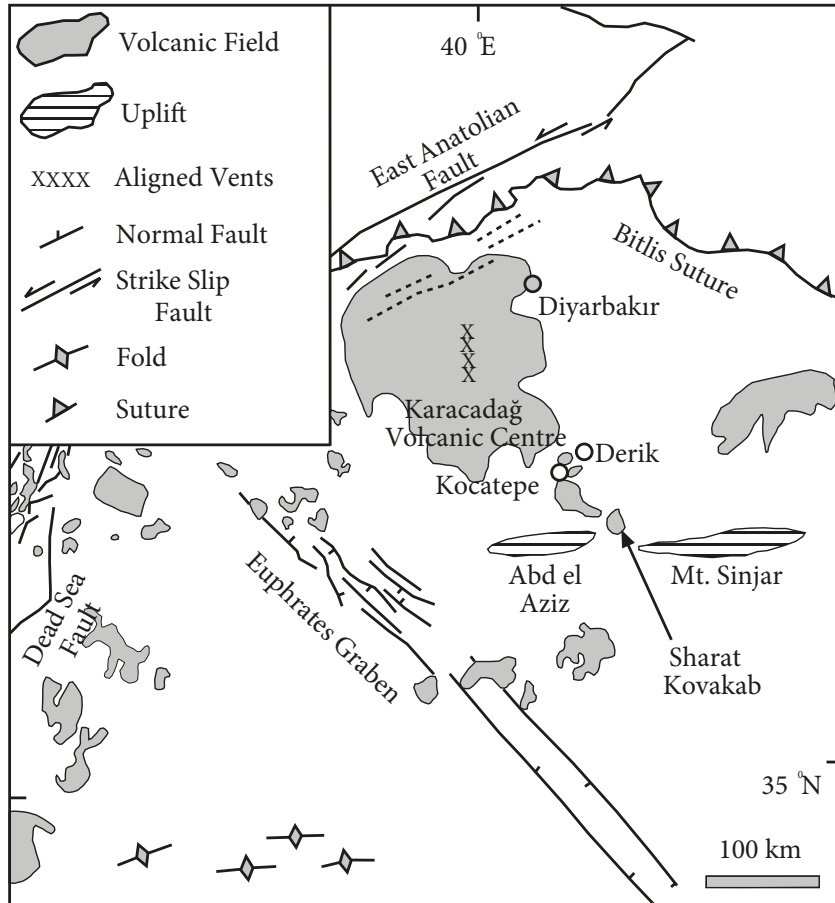


**Figure 2.** Location of the Karacadağ Volcanic Complex illustrating the axis of elongation of Mt. Karacadağ and sites of contemporaneous uplift at Sinjar and Abd el Aziz.

The Siverek plateau lavas cover a relatively large area (about 100 km<sup>2</sup>) and appear to have erupted from fissures with a NE–SW orientation (Ercan et al., 1990; Lustrino et al., 2010; Ekici et al., 2012). High <sup>87</sup>Sr/<sup>86</sup>Sr (>0.704) and low <sup>143</sup>Nd/<sup>144</sup>Nd (<0.51280) isotope ratios indicate that some Siverek magma interacted with the crust during transport towards the surface (Figure 4). However, cross-correlation with trace elements shows that most Siverek lavas escaped such interaction and their trace element variation resulted from polybaric melting of a relatively uniform mantle composition (Ekici et al., 2012) (Figure 5).

The Karacadağ Phase produced the main mass of Mt. Karacadağ. Ekici et al. (2014) used major and trace element ratios to distinguish three distinct magma types. Group K1 lavas have lower MgO (2.2–6.7 wt.%) and higher Al<sub>2</sub>O<sub>3</sub> (>15 wt.%) than K2 and K3 lavas. In groups K2 and K3, MgO is greater than 8 wt.%, but K3 is offset to lower SiO<sub>2</sub> and Al<sub>2</sub>O<sub>3</sub> and to higher TiO<sub>2</sub>, Fe<sub>2</sub>O<sub>3</sub>, Na<sub>2</sub>O, K<sub>2</sub>O, and P<sub>2</sub>O<sub>5</sub>. Lavas of group K2 are the most voluminous and were erupted along the length of the Mt. Karacadağ ridge.

Their trace element ratios indicate that these were mainly derived from partial melting of enriched lithospheric mantle at relatively shallow levels (Figure 5). The lavas of group K1 share many traits with group K2 but are more evolved. Ekici et al. (2014) demonstrated that group K1 could be produced by differentiation of K2 magma at approximately 5 MP depth, close to the boundary between the upper and lower crust. Lavas of group K3 are restricted to the central Mt. Karacadağ ridge.

The low <sup>87</sup>Sr/<sup>86</sup>Sr and high <sup>143</sup>Nd/<sup>144</sup>Nd ratios of K3 rocks led Ekici et al. (2014) to propose that this group contains a more substantial portion of melt derived from depleted mantle than K2. Furthermore, K3 trace element characteristics, such as enrichment of middle- and light-rare earth elements with respect to heavy rare earth elements, are compatible with their generation at greater depths than K2 magma (Figure 5).

The Ovabağ Phase is the youngest part of the KVC, and its products originated approximately 15 km to the east of Mt. Karacadağ, around the village of Ovabağ

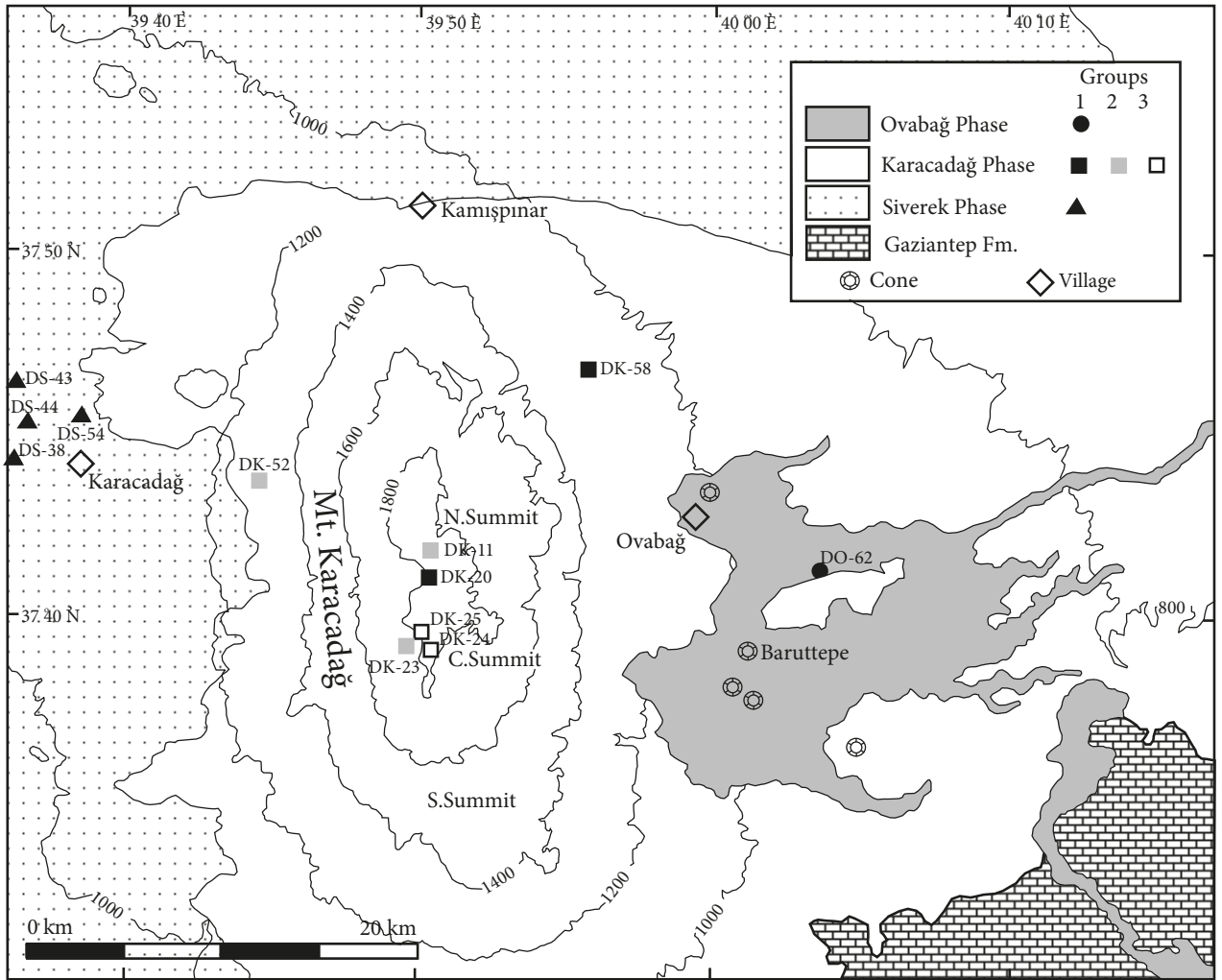


**Figure 3.** Map of different magma phases in the Karacadağ Volcanic Complex including the locations of lavas for which new Ar-Ar data are reported in this paper.

(Figures 2 and 3). These are predominantly alkali basalt flows that erupted from monogenetic cones overlying the products of the Karacadağ Phase. Individual Ovabağ lava flows extend eastward up to 20 km from the eastern flank of Mt. Karacadağ from where they were channelled into river valleys and flowed up to a further 5 km east or south-east (Figure 3). Ekici et al. (2014) recognised three different geochemical groups in the Ovabağ Phase, which resemble the Karacadağ Phase lavas in many ways. Ovabağ lavas contain more than 8 wt.% MgO and can be divided into three groups. O1 lavas have higher SiO<sub>2</sub> and Al<sub>2</sub>O<sub>3</sub> and lower CaO, Fe<sub>2</sub>O<sub>3</sub>, TiO<sub>2</sub>, K<sub>2</sub>O, and Na<sub>2</sub>O than O3 lavas at similar MgO. O2 lavas have the highest SiO<sub>2</sub> and lowest K<sub>2</sub>O, TiO<sub>2</sub>, and Na<sub>2</sub>O.

Group O3 are similar to group K3 (Ekici et al., 2014), although their rare earth systematics suggest a somewhat

shallower mantle source (Figure 5). Trace elements in group O1 closely resemble those of group K2, indicating a shallow, probably lithospheric, mantle source (Figure 5). Finally, the only substantive difference between groups O2 and O1 is the slightly lower concentration of incompatible element contents in O1 lavas, suggesting that they formed through slightly higher degrees of partial melting (Ekici et al., 2014).

The findings of detailed investigations of the three KVC phases by Ekici et al. (2012, 2014) are summarised in Figure 6, which also includes data from other relevant studies (Keskin et al., 2012b; Lustrino et al., 2012). Data for group K1 have been omitted because these are more evolved, which may obscure parental melt compositions. In this plot, the <sup>143</sup>Nd/<sup>144</sup>Nd isotope ratio is a proxy for the degree of chemical depletion of the mantle or the extent

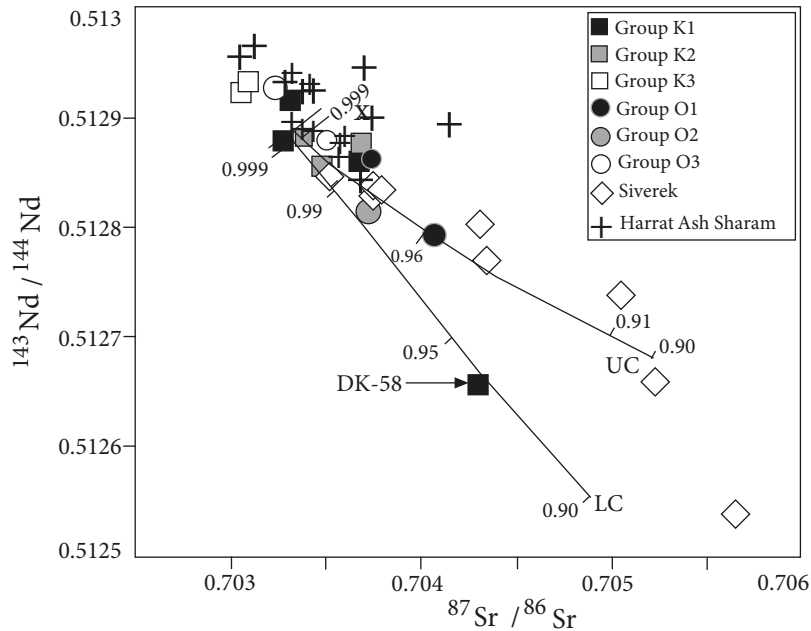


**Figure 4.** Plot of  $^{87}\text{Sr}/^{86}\text{Sr}$  versus  $^{143}\text{Nd}/^{144}\text{Nd}$  for lavas from the Karacadağ Volcanic Complex and Harrat Ash Shaam. Black curves illustrate models of assimilation with fractional crystallisation for contamination by upper (UC) and lower (LC) crust. Figures indicate fraction of melt remaining. Details of these models were presented by Ekici et al. (2012).

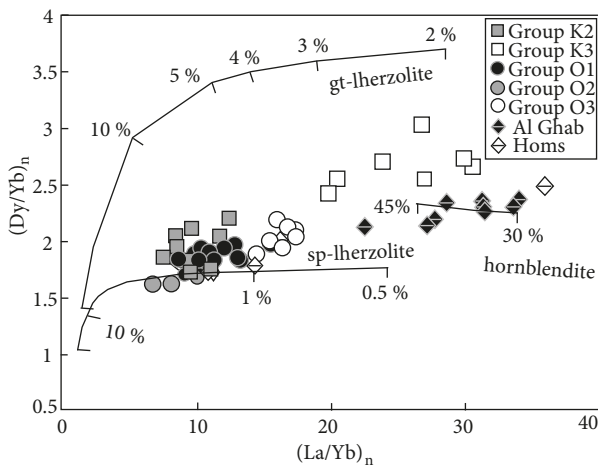


**Figure 5.** Plot of Dy/Yb versus La/Yb for lavas from the Karacadağ Volcanic Complex. Groups distinguished based on wider geochemical criteria as described in text. The variations of both ratios in each group suggest melting over a range of depths, but groups K2, O1, and O2 contain greater proportions of melts from shallower levels. The displacement to lower La/Yb indicates that Karacadağ (K) Phase lavas represent higher degrees of melting than Ovabağ (O) Phase magma. Group K1 is omitted because these lavas are more evolved than those of the other groups. Model curves for melting of garnet (gt-)lherzolite and spinel (sp-)lherzolite are from Ekici et al. (2014).

of crustal contamination. Values of  $^{143}\text{Nd}/^{144}\text{Nd}$  of about 0.51300 represent lavas derived from relatively depleted mantle (Ekici et al., 2014). Lower  $^{143}\text{Nd}/^{144}\text{Nd}$  values can represent magma derived from mantle heterogeneity. Comparing lavas from the KVC with other sites in the region suggests that such mantle heterogeneity can produce magma with  $^{143}\text{Nd}/^{144}\text{Nd}$  ratios down to values of 0.51280. However, Ekici et al. (2012) showed that Siverek Phase lavas with  $^{143}\text{Nd}/^{144}\text{Nd}$  ratios lower than 0.51280 are likely to contain a substantial contribution from crustal contamination. This is also likely to be the case for Karacadağ Phase lavas with low  $^{143}\text{Nd}/^{144}\text{Nd}$  (Ekici et al., 2014). Thus, the two grey ellipses in Figure 6 represent ranges for the two probable end-member compositions of KVC mantle sources (Ekici et al., 2014).

Dy/Yb can be used as a depth-sensitive probe of melting, assuming peridotitic sources with spinel or garnet as the aluminous phase. In this case, higher Dy/Yb values represent a greater role for melts derived at greater garnet-bearing depth (Baker et al., 1997). Thus, the data are consistent with a range of sources between a deep, more-depleted (i.e. high  $^{143}\text{Nd}/^{144}\text{Nd}$ ) mantle end-member and a shallower, less-depleted end-member. The former is consistent with the range of compositions found in the asthenospheric sources of MORB, while the latter resembles lithospheric sources previously advocated for as

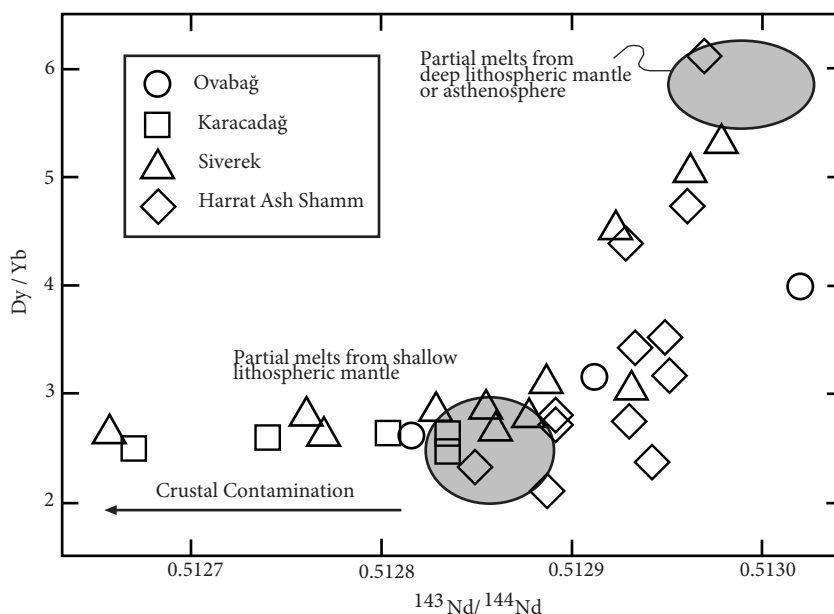


**Figure 6.** Plot of  $^{143}\text{Nd}/^{144}\text{Nd}$  versus  $\text{Dy}/\text{Yb}$  for lavas from the Karacadağ Volcanic Complex (data from Ekici et al., 2012, 2014; Lustrino et al., 2012; Keskin et al., 2012b). Group K1 is omitted because these lavas are more evolved than those of other groups. Harrat Ash Shaam data (Shaw et al., 2003) plotted for comparison. Grey ellipses indicate approximate composition of inferred shallow lithospheric and deep asthenospheric components. Crustal contamination displaces  $^{143}\text{Nd}/^{144}\text{Nd}$  towards lower values, as indicated by the black arrow.

the Northern Arabian Plate (Baker et al., 1997; Shaw et al., 2003; Ekici et al., 2014).

### 3. Samples and analysis

The lavas used in this study were described by Ekici et al. (2012, 2014). Representative samples were chosen for  $^{40}\text{Ar}/^{39}\text{Ar}$  geochronology from the Siverek, Karacadağ, and Ovabağ phases of activity (Table; Figures 3 and 7) based on the freshness and grain size of potassium-bearing minerals. Whole-rock basalt, trachybasalt, and tephrite samples were crushed, sieved, and cleaned in an ultrasonic bath. Between 20 and 50 mg of purified rock powder with grain sizes of  $<250\ \mu\text{m}$  were loaded into aluminium-foil packets. These were irradiated at the McMaster Nuclear Reactor in two batches in the 5C position for 26.5 h with an approximate neutron flux of  $10^{18}\ \text{cm}^{-2}\ \text{s}^{-1}$ . Irradiation interference on K, Ca, and Cl was corrected by irradiating and analysing KCl and  $\text{CaF}_2$  pure salts. J factors were estimated by use of duplicate measurements of the Fish Canyon sanidine standard with an age of 28.02 Ma (Renne et al., 1998). For these analyses, J values of 0.009035 and 0.009239 were determined for each irradiation vessel, respectively, and used with a relative error of 1.2%.

Argon isotopic analyses were conducted at the University of Montpellier using the apparatus and

protocol described by Garcia et al. (2003). Samples in their aluminium packets were loaded into a double vacuum Staudacher type furnace. Classical furnace step heating was conducted in thirteen or fourteen steps from 500 °C to 1400 °C with temperature monitored by a thermocouple. Gases were purified using cold traps with liquid air and Al-Zr getters. Once cleaned, the gas was introduced into a VG3600 mass spectrometer and allowed to equilibrate for 2 min prior to analysis in static mode. Signals were measured by the mean of a Faraday cup with a  $10^{11}$  ohm resistor for  $^{40}\text{Ar}$  and  $^{39}\text{Ar}$ , and by a photomultiplier after interaction on a Daly plate for  $^{39}\text{Ar}$ ,  $^{38}\text{Ar}$ ,  $^{37}\text{Ar}$ , and  $^{36}\text{Ar}$ . Gain between the collectors was estimated by duplicate analysis of  $^{39}\text{Ar}$  on both collectors during each analysis, and also by statistical analysis over a period of several years. This gain is 50 and is known at better than 1.5%. This error is included in the age calculation, along with analytical errors on each signal and errors on the blank values that were calibrated before every sample analysis for 500 °C, 1000 °C, and 1200 °C. Errors on age determinations are quoted as 1 standard deviation.

Ages determined from age spectra are weighted mean plateaus (Fleck et al., 1977) or simple mean ages in the cases where subsequent steps either overlap at the  $1\sigma$  level or the total  $^{39}\text{Ar}$  cumulated from these steps is insufficient

**Table.** Ar-Ar ages measured for Siverek (DS), Karacadağ (DK), and Ovabağ (DO) phase lavas of the Karacadağ Volcanic Complex. Where plateau and isochron ages differ, the preferred age is given in ordinary type face.

Plateau				Isochron								Remarks
Sample	Group	Total steps	age	s.d.	# steps used	age	s.d.	MSWD	$^{40}\text{Ar}/^{36}\text{Ar}_i$	s.d.	# steps used	
DS-44		11	18.93	1.67	2	-						Two steps contained majority of gas
DS-54		13				11.10	1.05	9	303	5	10	Excess Ar present
DS-38		13	7.39	0.43	1	-						Single step contained majority of gas
DS-43		14	6.99	0.18	6	6.60	0.54	10.3	304	8	6	
						-						
DK-24	K3	13	4.10	0.10	4	4.50	0.12	7	303	4	10	
DK-11	K2	13	2.80	0.30	3	2.10	0.31	3	309	3	10	Excess Ar present
DK-52	K2	13	-			1.67	0.52	0.9	312	3	10	
DK-25	K3	13	-			1.41	0.20	7	303	3	12	
DK-20	K1	13	1.00	0.10	5	1.16	0.27	10	308	7	7	
DK-58	K1	13	1.10	0.10	2	0.99	0.22	10	313	6	9	
DK-23	K2	13	-			0.91	0.11	5	297	3	9	
DO-62		13	-			0.29	0.13	6	310	6	8	Excess Ar present

to define a classical plateau. All errors from age spectra take the error on the J factor into account. However, the plateau criterion was rarely achieved, notably for the younger rocks, in which case ages were determined from an inverse isochron diagram of  $^{36}\text{Ar}/^{40}\text{Ar}$  versus  $^{39}\text{Ar}/^{40}\text{Ar}$  (Roddick et al., 1980) that allows homogeneous excess components to be individualised on many occasions. Errors on age and intercept age include individual errors on each point and linear regression by the method of York (1969). The goodness of fit relative to individual errors was measured by mean square weighted deviation (MSWD).

#### 4. Petrography

The lavas from the KVC are all mildly alkaline, and the majority are very fresh with little alteration. Lavas from the Siverek Phase contain olivine, plagioclase, and augite phenocrysts, and are predominantly basalts, trachybasalts, and tephrites. Olivine is the main phenocryst phase in Karacadağ Phase lavas, which include basalt, trachybasalts, tephrites, basanite, and phonotephrites. Ovabağ Phase lavas include basalts, alkali basalts, trachybasalts, and rare tephrites, and they have olivine phenocrysts, augite, and titanite microliths. Olivine is occasionally partially iddingsitized (Figure 8a), while clinopyroxene is generally titanium-rich and the groundmass usually contains Fe-Ti oxides (Figure 8b). Plagioclase phenocrysts display oscillatory zoning (Figure 8c) and some indicate signs of disequilibrium with the presence of sieve textures (Figure

8d). Such disequilibrium might arise from magma mixing or crustal contamination (Dungan and Rhodes, 1978), but could also result from decompression or heating (Nelson and Montana, 1992; Thy et al., 2013).

The KVC lavas do not contain xenoliths or xenocrysts; however, the isotopic and trace element compositions show evidence of crustal contamination of some magmas (Ekici et al., 2012, 2014).

#### 5. Results

The plateau and reverse isochron ages determined for twelve whole-rock KVC lavas are reported in the Table and Figure 7.

##### 5.1. Siverek Phase

Four analyses were conducted on Siverek Phase lavas. Sample DS-38 yielded very little gas until fusion and so the age ( $7.39 \pm 0.43$  Ma) is, in effect, a total fusion age. This is indistinguishable from the plateau age for DS-43 ( $6.99 \pm 0.18$  Ma), which was preferred to the isochron age due to the elevation of MSWD in the latter. These two ages are for samples from the western part of the Siverek field and correspond to similar K/Ar ages of approximately 6.7 Ma for lavas from this area reported by Lustrino et al. (2010) and Keskin et al. (2012a). The two remaining samples gave older ages, albeit with poorer precision. The age profile of releases from DS-44 fluctuated significantly, but 65% of the gas was released from two adjacent steps giving an age

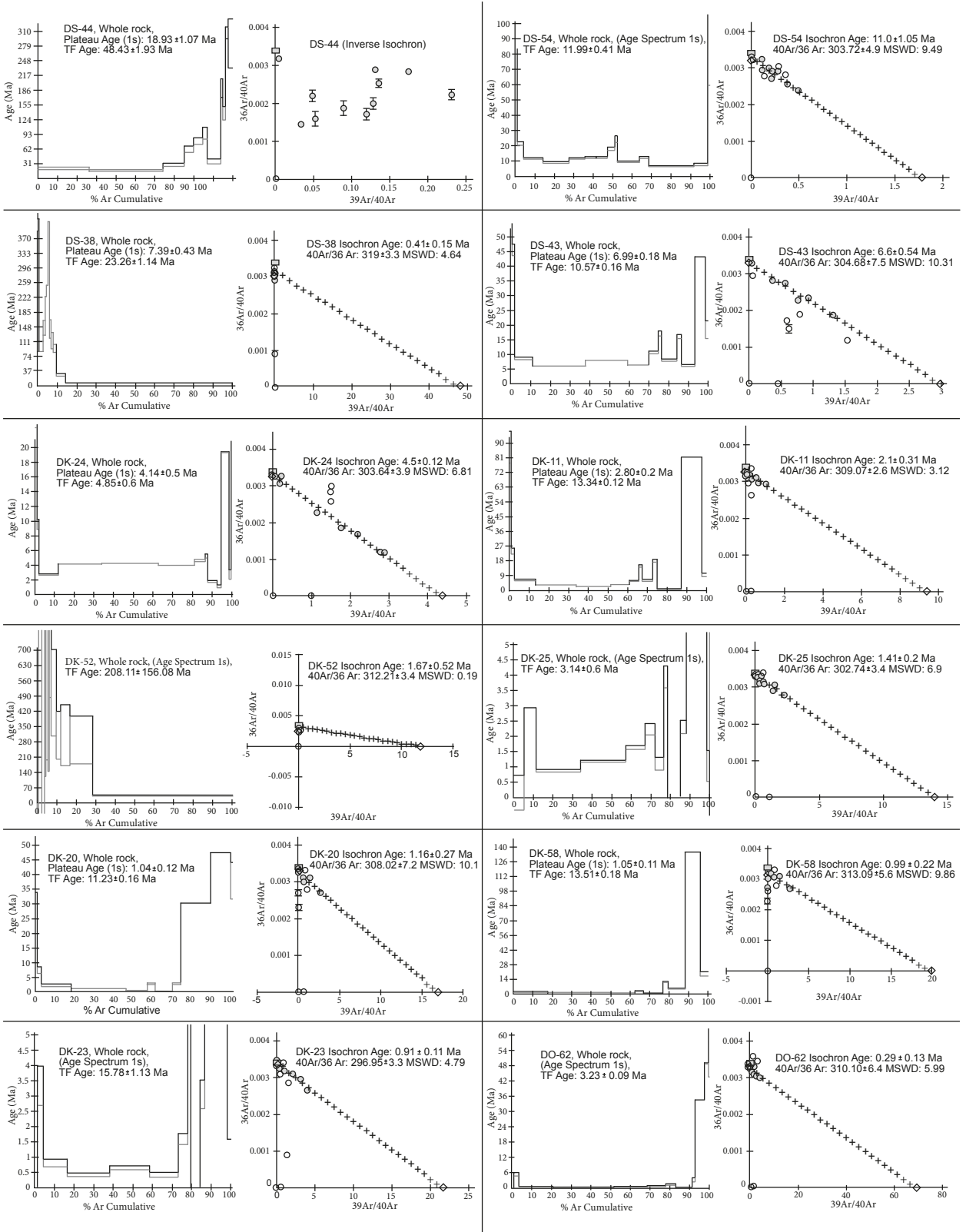
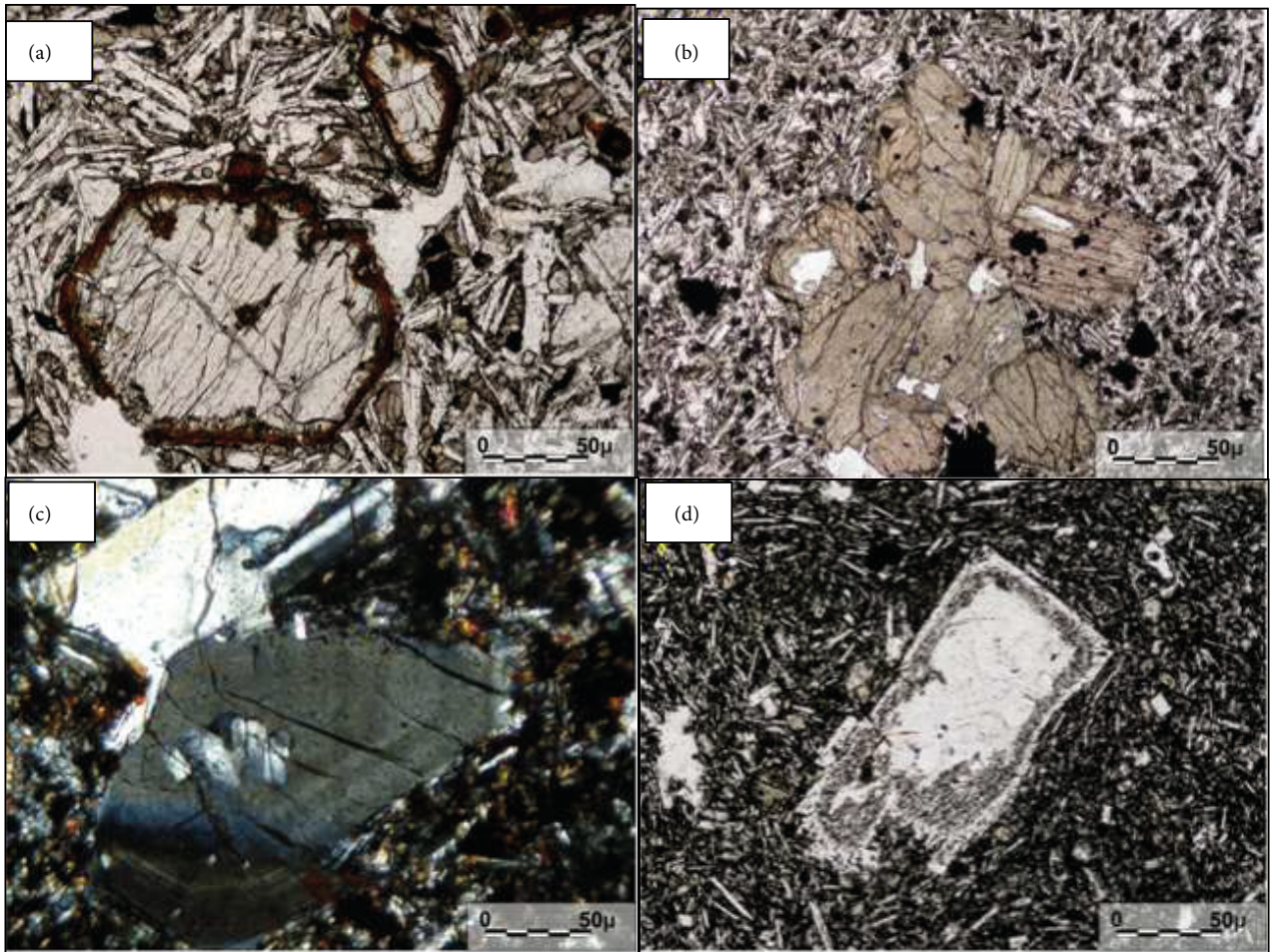


Figure 7. Ar-Ar step-heating and isochron age of Karacadağ Volcanic Complex.



**Figure 8.** Photomicrographs of thin sections of rocks from Karacadağ Volcanic Complex. a) Presence of iddingsite in olivine in plane-polarised light. b) Titanium-rich and Fe-Ti oxides in clinopyroxene in plane-polarised light. c) Oscillatory zoning texture in plagioclase in cross-polarised light. d) Presence of sieve texture in plagioclase in plane-polarised light.

of  $18.93 \pm 1.67$  Ma. DS-54 did not give a stable plateau but yielded an isochron age of  $11.10 \pm 1.05$  Ma. The latter of these is similar to 10–11 Ma K/Ar ages reported by Ercan et al. (1990) and Haksal (1981).

### 5.2. Karacadağ Phase

Seven analyses were conducted on the three subgroups of the Karacadağ Phase. In group K1, the isochron ages for lavas DK-20 ( $1.16 \pm 0.27$  Ma) and DK-58 ( $0.99 \pm 0.22$  Ma) are of slightly superior quality to, but within the analytical uncertainty of, plateau ages. Three lavas from group K2 gave isochron ages that overlap with those of group K1. DK-23 returned  $0.91 \pm 0.11$  Ma and DK-52 yielded  $1.67 \pm 0.52$  Ma, while the isochron age for DK-11 is  $2.10 \pm 0.31$  Ma. DK-52 also yielded a short plateau at  $2.08 \pm 0.30$  Ma. Two ages were obtained from lavas of group K3. The isochron age of  $1.41 \pm 0.20$  Ma for DK-25 lies within the range measured for groups K1 and K2. For DK-24, the

isochron age of  $4.50 \pm 0.12$  Ma suggests that this lava is slightly older than any of the other Karacadağ Phase lavas analysed either in this work or previously (Keskin et al., 2012a and references therein).

### 5.3. Ovabağ Phase

Our dataset contains a single new analysis from the Ovabağ Phase. The youth of these rocks makes their analysis more challenging, but sample DO-62 gave an isochron age of  $0.29 \pm 0.13$  Ma, which is within the uncertainty of K/Ar measurements (Keskin et al., 2012a) and is consistent with the freshness of these flows.

## 6. Discussion

The KVC experienced two major transitions, first from plateau-style magmatism (Siverek Phase) to a focussed volcanic ridge (Karacadağ Phase), and then to discrete monogenetic events (Ovabağ Phase). We have previously

discussed that lithospheric shear generated the Siverek Phase of magmatism as the Arabian Plate drifted north (Ekici et al., 2012) and that the transition to a more focussed axis was associated with stress that developed due to proximity to the Arabian–Anatolian collision (Ekici et al., 2014). The geochronological data allow us to explore the relationship between magmatism and collisional stress in more detail.

### 6.1. Onset of Siverek magmatism

Keskin et al. (2012a and references therein) used K/Ar dating to develop the most detailed evolutionary model for the KVC to date. They proposed that Siverek plateau lavas comprised at least two pulses of activity at 10–11 Ma and at ~6.7 Ma. Our new data are consistent with volcanism occurring in both these periods (Table). The oldest age we obtained was  $18.93 \pm 1.67$  Ma for sample DS-44. This is substantially older than any previous measurements for the Siverek Phase. It is possible that this analysis may be affected by excess argon and so it could represent a maximum estimate. However, even allowing for uncertainty on this measurement, this is still sufficient to suggest that the Siverek Phase was active as early as 17 Ma during the Middle Miocene, and possibly the Early Miocene.

### 6.2. Timescales of Karacadağ development

Keskin et al. (2012a) proposed that Karacadağ Phase magmatism proceeded through different types of eruptive activity. They found that at ~3.9 Ma, lava plateaux and pyroclastic flows formed to the east and south of the site of the Karacadağ ridge. These were then capped by lava flows at ~2.7 Ma. Finally, the Karacadağ ridge emerged at ~1.7 Ma and grew over the subsequent 700 ka. Our sample DK-24, which lies on the central part of the ridge (Figure 3), gave an age of  $4.5 \pm 0.12$  Ma (Table; Figure 7). This suggests that parts of the ridge may have been volcanically active and built substantial volume earlier than previously thought. Our remaining analyses reinforce the idea that there was an upsurge in activity on the ridge at ~2 Ma and that the bulk of the ridge was constructed between then and 1 Ma (Figure 9).

With respect to the different geochemical groups of the Karacadağ Phase, the geochronology data show that rocks from groups K3 and K2 were both generated during the early stages of the Karacadağ Phase (Table). As noted above, group K3 lava DK-24 was the oldest Karacadağ Phase lava that we found, and all other rocks produced prior to 1.4 Ma belong to either group K2 or K3. Lavas from group K1 formed by differentiation of K2-type magma at the boundary of the upper and lower crust (Ekici et al., 2014). The two  $^{40}\text{Ar}/^{39}\text{Ar}$  analyses of K1 lavas gave ages of <1.2 Ma. If these two ages are representative of the whole K1 group, then this suggests that the conditions to allow differentiation of this more evolved group of basalts

only developed during the later stages of the Karacadağ Phase. This may be because the crustal tension required to accommodate large volumes of more evolved melt only developed later, during the history of the fissure volcano.

### 6.3. Mt. Karacadağ as an expression of melt transport in a stressed foreland

Mt. Karacadağ is the most conspicuous volcanic feature of the KVC, with an axis lying subparallel to the convergence between Arabia and Anatolia (Figures 2 and 3). This alignment has been attributed to tension generated when extension due to westward escape of Anatolia along the east Anatolian Fault was transmitted into weak parts of the Arabian crust (Adiyaman and Chorowicz, 2002). In contrast, Keskin et al. (2012b) favoured a hotspot or upwelling of mantle that resembled the Afar plume. However, Ekici et al. (2014) demonstrated that the Pb isotopes systematic of KVC lavas are not compatible with involvement of the Afar plume or any other hotspot component that has been postulated for the Northern Arabian Plate.

While tensional stress may have been generated by nearby faults, we propose an alternative origin for the lithospheric weakness expressed by the Mt. Karacadağ ridge between 4 and 1 Ma. The near orthogonal collision of Arabia with Anatolia produced compressive stress in the northern Arabian lithosphere with the principal compression direction ( $\sigma_1$ ) oriented approximately north–south, parallel to the orientation of the convergence (Figure 2). Magma pathways would open due to tension in the  $\sigma_3$  direction, in this case east–west. Therefore, the pathways themselves would be elongated parallel to  $\sigma_3$ . Thus, magma traversing the crust beneath Mt. Karacadağ is likely to have been channelled through a system of crustal fissures aligned north–south, parallel to the main convergence vector. This is similar, in principle, to the formation of regional dyke swarms in which individual intrusive bodies are oriented perpendicular to the direction of extension. In this case, however, the mechanism driving the formation of magma pathways through the crust is lithospheric compression parallel to the fissure system, rather than extension perpendicular to it. This is similar to the mechanism of parasitic cone formation on arc volcanoes envisaged by Nakamura (1977).

Independent evidence for compression of the northern Arabian lithosphere at this time is provided by the Abd el Aziz and Sinjar anticline structures, which lie approximately 100 km to the south of Mt. Karacadağ (Figure 2). Both anticlines are elongated east to west, inferring north–south compression, due to Late Cretaceous normal faults being reactivated as thrust during the Plio–Pleistocene (Brew et al., 1999). Brew et al. (1999) used the absence of deformation in some Pliocene strata to infer that this reactivation started no earlier than 3 Ma. The combined

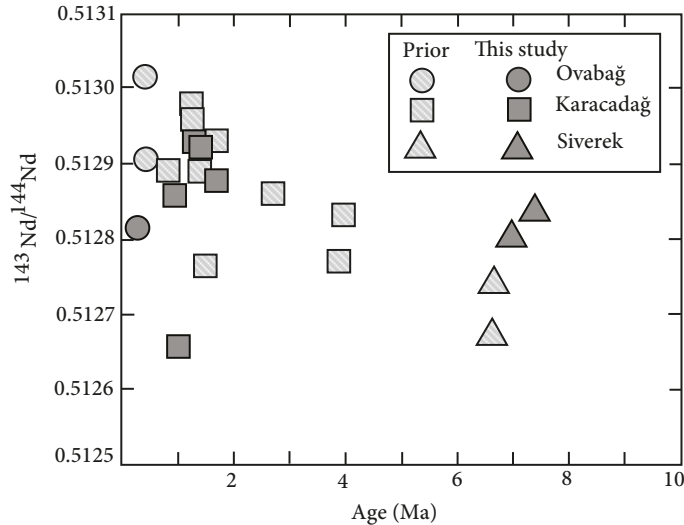


**Figure 9.** Plot of  $^{143}\text{Nd}/^{144}\text{Nd}$  versus age for lavas from the three phases of the Karacadağ Volcanic Complex. Pale symbols are Ar-Ar data from this work; closed symbols are published K-Ar dates. Data from Pearce et al. (1990), Ekici et al. (2012, 2014), Lustrino et al. (2012), and Keskin et al. (2012b). Group K1 omitted because these lavas are more evolved than those of other groups. Error bars of  $2\sigma$  are plotted or are smaller than symbols.

geochronology datasets (Figure 9) indicate that strongly aligned volcanism at Mt. Karacadağ became predominant at 1.7–2.0 Ma. Thus, the development of north–south magmatic alignment at Mt. Karacadağ is contemporaneous with the nearby north–south vergent anticlines at Abd el Aziz and Sinjar.

We note that the Abd El Aziz and Sinjar anticlines are separated by a small volcanic field at Sharat Kovakab. Although its activity appears to have been contemporaneous with the Ovabağ Phase (Al-Kwatli et al., 2014) rather than the Karacadağ Phase, subsidiary cones at Sharat Kovakab occur to the NNE and SSW of the main Tel Kovakab structure. This is subparallel to both the vergence direction inferred by the anticlines and the Arabia–Eurasia plate margin. This provides further evidence that compression of the Arabian foreland caused Quaternary volcanic feeder systems to align parallel to the direction of  $\sigma_1$ .

Another example of convergence alignment of magmatism can be observed in the northern Fly Platform of the New Guinea foreland. The Bosavi volcano is a large stratovolcano immediately adjacent to the southern margin of the Papuan Thrust and Fold Belt. This volcanic system erupted alkali olivine basalt, trachybasalt, tholeiite, basalt, and andesite with relatively low silica (Mackenzie and Johnson, 1984; Davies, 1990). Davies (1991) noted that the main cone of Bosavi lies closest to the collision zone but a chain of eruptive centres is aligned SW of

the main cone, towards the interior of the foreland. A tear fault, the Bosavi Lineament, parallel to this feature and displaced by only a few kilometres, provides further evidence of disruption of the leading edge of the foreland (Hill et al., 2010). Like Mt. Karacadağ, the alignment of volcanism is subparallel to convergence while the mafic nature of Bosavi lavas indicates that magma originated in the mantle. Therefore, we identify this as another example of magmatism aligning with compression of continental foreland lithosphere in a young orogenic belt.

#### 6.4. Ovabağ Phase magmatism

Our single age determination for an Ovabağ Phase lava of  $0.29 \pm 0.13$  Ma is indistinguishable from K/Ar ages of 0.42 and 0.39 Ma reported by Keskin et al. (2012a). Thus, we concur with their conclusion that the Ovabağ magmatism occurred towards the end of the Quaternary period. However, Ekici et al. (2014) identified that the same range of mantle sources contributing to Ovabağ were active throughout the Karacadağ Phase (Figures 4–6). Thus, the progression from a strongly aligned fissure system at  $\geq 1$  Ma to discrete, monogenetic cones at  $\leq 0.5$  Ma did not reflect a substantial change in the sources contributing to KVC magmatism.

Volcanic vents of the Ovabağ Phase are dispersed across the low plain to the east of Mt. Karacadağ (Figure 3). Further small cones of similar size are found to the SE of Mt. Karacadağ between the towns of Kocatepe and Derik (Figure 2). This broad distribution indicates that

these monogenetic eruptions occurred after dissipation of the strongly focussed stress field in southern Turkey that produced the Mt. Karacadağ shield volcano. Therefore, we suggest that the peak of fissure activity in the Karacadağ Phase represents the time of maximum compressive stress at the nose of the Arabian–Anatolian collision. In turn, the upsurge in fissure volcanism at ~2 Ma and transition to disperse activity at <0.5 Ma suggests that strongly aligned stress fields can develop and then dissipate over less than 1.5 million years.

### 6.5. Evolution of KVC mantle sources

Lustrino et al. (2010) and Keskin et al. (2012b) both suggested that the sources of KVC lavas became more “depleted” over time. To support this claim they presented  $^{143}\text{Nd}/^{144}\text{Nd}$  data that tended towards higher values in progressively younger rocks (grey symbols labelled “Prior” in Figure 9). This trend was strongly influenced by the relatively low  $^{143}\text{Nd}/^{144}\text{Nd}$  of two Siverek Phase lavas at 6.5 Ma and relatively high  $^{143}\text{Nd}/^{144}\text{Nd}$  of one Ovabağ Phase lava. Without these samples, the change in the  $^{143}\text{Nd}/^{144}\text{Nd}$  over time is much less pronounced. Combining our new geochronological dataset with findings from the studies of Ekici et al. (2012, 2014) allows us to evaluate this proposition further.

Ekici et al. (2012) found that the primary cause of isotopic variation in Siverek Phase rocks was contamination of magma by the crust through which it was transported. This produced higher  $^{87}\text{Sr}/^{86}\text{Sr}$  and lower  $^{143}\text{Nd}/^{144}\text{Nd}$  in the most affected rocks (Figure 4). As discussed above (Section 2.2; Ekici et al., 2012), our prior investigation of the Siverek lavas led us to attribute any  $^{143}\text{Nd}/^{144}\text{Nd}$  ratios lower than 0.51280 to interaction with the crust (Figure 6). This is also consistent with other studies of northern Arabian intraplate magmatism, e.g., Harrat Ash Shaam (Shaw et al., 2003), which indicate a more limited range of  $^{143}\text{Nd}/^{144}\text{Nd}$  values in the mantle than the range inferred by Lustrino et al. (2010) and Keskin et al. (2012b). The older end of the “Prior” secular trend in Figure 9, based on K–Ar geochronological data, is anchored by two Siverek lavas with  $^{143}\text{Nd}/^{144}\text{Nd}$  lower than 0.51280. Our detailed study of Siverek magmatism (Ekici et al., 2012) showed the compatibility between our data and these other Siverek datasets and thus, based on our findings in that work, we attribute the low neodymium isotope ratios of these lavas to crustal contamination.

Isotopic and trace element data (Ekici et al., 2012) show that the two Siverek lavas for which we obtained Ar–Ar ages experienced negligible crustal contamination. As such, these analyses represent a better estimate of the mantle source of the Siverek magmatism. Their  $^{143}\text{Nd}/^{144}\text{Nd}$  ratios (dark symbols in Figure 9) are notably higher than those reported by Lustrino et al. (2010) and Keskin et al. (2012b) and disrupt the older part of the putative “Prior” trend in  $^{143}\text{Nd}/^{144}\text{Nd}$  versus age (Figure 9). As our new data

values lie within the range of values inferred for the mantle sources of the subsequent phases of the KVC, we infer that the same range of sources available to the KVC were also available to the Siverek magmatism.

Like the Siverek lavas, some Karacadağ Phase rocks also possess  $^{143}\text{Nd}/^{144}\text{Nd} < 0.51280$  (with associated elevated  $^{87}\text{Sr}/^{86}\text{Sr}$ ) that, again, may result from crustal contamination (Figures 4 and 6). In general, however, Ekici et al. (2014) concluded that the importance of crustal contamination decreased from Siverek to Karacadağ magmatism. As noted by Lustrino et al. (2012) and Keskin et al. (2012a), Karacadağ Phase lavas display some of the most elevated  $^{143}\text{Nd}/^{144}\text{Nd}$  ratios among all KVC rocks, but this phase does display a range of  $^{143}\text{Nd}/^{144}\text{Nd}$  values in the period from 1 to 2 Ma (Figure 9). Elevated  $^{143}\text{Nd}/^{144}\text{Nd}$  ratios are most likely to represent an increased contribution from depleted, asthenospheric mantle (Ekici et al., 2014). Thus, we concur with Keskin et al. (2012b) that the role of asthenospheric sources is apparent in the isotopic data for the later products of the Karacadağ Phase (i.e. <2 Ma). However, we do not agree that this is a simple evolution from lithosphere-dominated to asthenosphere-dominated melts. We interpret KVC magmatism as being derived from both the asthenosphere and lithosphere for three principal reasons. First, the wide range of  $^{143}\text{Nd}/^{144}\text{Nd}$  and trace element ratios displayed by the Karacadağ Phase indicates contributions from both deep and shallow sources (Figures 5 and 6). Second, as noted previously, the oldest age we measured for Karacadağ Phase lava was 4.5 Ma (DK-24), and this is a member of group K3. Although isotopic ratios were not measured for this sample, the trace element chemistry of group K3 lavas indicates asthenospheric sources (Ekici et al., 2014). Third, the highest  $^{143}\text{Nd}/^{144}\text{Nd}$  of any KVC magmatism in the “Prior” trend of Figure 9 comes from the Ovabağ Phase. However, consideration of all Ovabağ lavas shows that they display as wide a range of  $^{143}\text{Nd}/^{144}\text{Nd}$  as the Karacadağ Phase (Figure 4), further disrupting the “Prior” trend. Therefore, we do not regard the isotopic data in Figure 9 as showing a simple temporal trend from low  $^{143}\text{Nd}/^{144}\text{Nd}$  to high  $^{143}\text{Nd}/^{144}\text{Nd}$  in primary magmas. Instead, we interpret the low values present in older lavas (>5 Ma) to reflect a greater role for crustal contamination, superimposed on a range of primary melts with contributions from both asthenospheric and lithospheric sources. Both of these mantle sources contributed to magmatism throughout the rest of the KVC activity, perhaps with slightly greater contribution from the asthenosphere, but not to the significant exclusion of the lithosphere.

## 7. Conclusions

New  $^{40}\text{Ar}/^{39}\text{Ar}$  data for the three phases of the KVC help elucidate its evolution. The Siverek Phase started producing plateau basalts at least ~17 million years ago rather than

11 Ma, as has been proposed previously. A strong phase of activity occurred in the western KVC close to 7 Ma. There was then a hiatus before the first recorded activity of Mt. Karacadağ at ~4.5 Ma. Between 2 and 1 Ma, the lithosphere of Mt. Karacadağ experienced a strong north-south compression, associated with the Arabia-Anatolia collision, allowing repeated transport and eruption of melt generated in the lithospheric and asthenospheric mantle. This activity coincided with structural inversion ~100 km to the south, where the Abd el Aziz and Sinjar structures were uplifted with  $\sigma$  oriented in the same direction at the Mt. Karacadağ fissure system. The youngest KVC magmatism of the Ovabağ Phase is more dispersed, suggesting dissipation of the stress field subsequent to 1 Ma. At that time, there was still sufficient stress in the lithosphere to the south to align volcanic vents of Sharat Kovakab between Abd el Aziz and Sinjar.

We propose that the formation of the elongated Mt. Karacadağ shield volcano was the result of a compressional stress field (Nakamura, 1977). Although this mechanism could produce tension to open melt pathways through the lithosphere, it provides limited scope for mantle melting to occur through upwelling, as postulated beneath rifts and other mantle thin-spots (McKenzie and Bickle,

1988). Furthermore, contributions from asthenospheric melts were not limited to any particular time during the history of the KVC. Therefore, it is not possible to attribute asthenospheric melting only to the mechanism that resulted in the fissure volcano.

Hirano et al. (2006) and Sifré et al. (2014) suggested that incipient melts are widespread in shallow oceanic asthenosphere and can exploit fractures or other structures to form small intraplate volcanic provinces. Such melts should also be anticipated to exist beneath continental lithosphere, where they would be available for transport to the surface wherever and whenever tension opens pathways through the lithosphere. We interpret Mt. Karacadağ as an extreme example of focused transport of melt from the asthenosphere in a continental setting, but one that also demonstrates that lithospheric material can contribute to the magma that reaches the surface.

### Acknowledgements

We acknowledge the financial support of TÜBİTAK (project no. 107Y025) to conduct fieldwork and analytical phases of this work. Colin Macpherson is grateful to Durham University for a period of research leave during the preparation of this work.

### References

- Adiyaman Ö, Chorowicz J (2002). Late Cenozoic tectonics and volcanism in the northwestern corner of the Arabian plate: a consequence of the strike-slip Dead Sea fault zone and the lateral escape of Anatolia. *Journal of Volcanology and Geothermal Research* 117: 327-345.
- Al-Kwatli MA, Gillot PY, Lefevre JC, Hildenbrand A, Kluska JM (2014). Magma genesis controlled by tectonic styles in the northern part of the Arabian plate during Cenozoic time. In: Rollinson HR, Searle MP, Abbasi IA, Al-Lazki A, Kindi MH (editors). *Tectonic Evolution of the Oman Mountains*. London, UK: Geological Society of London Special Publications, pp. 61-91.
- Allen M, Jackson J, Walker R (2004). Late Cenozoic reorganization of the Arabia-Eurasia collision and the comparison of short-term and long-term deformation rates. *Tectonics* 23: TC2008.
- Baker JA, Menzies MF, Thirlwall MF, Macpherson CG (1997). Petrogenesis of quaternary intraplate volcanism, Sana'a, Yemen: implications for plume-lithosphere interaction and polybaric melt hybridization. *Journal of Petrology* 38: 1359-1390.
- Bosworth W, Huchon P, McClay K (2005). The Red Sea and Gulf of Aden Basins. *Journal of African Earth Sciences* 43: 334-378.
- Brew G, Litak R, Baranzangi M, Sawaf T (1999). Tectonic evolution of Northeast Syria: regional implications and hydrocarbon prospects. *Geo Arabia* 4: 289-318.
- Brigland D, Demir T, Seyrek A, Pringle M, Westaway R et al. (2007). Dating Quaternary volcanism and incision by the River Tigris at Diyarbakır, SE Turkey. *Journal of Quaternary Sciences* 21: 437-455.
- Demir T, Westaway R, Brigland D, Pringle M, Yurtmen S et al. (2007). Ar-Ar dating of late Cenozoic basaltic volcanism in northern Syria: implications for the history of incision by the River Euphrates and uplift of the northern Arabian Platform. *Tectonics* 26: TC3012.
- Dungan MA, Rhodes MJ (1978). Residual glasses and melt inclusions in basalts from DSDP legs 45 and 46: evidence for magma mixing. *Contributions to Mineralogy and Petrology* 67: 417-431.
- Ekici T, Macpherson CG, Otlı N (2012). Polybaric melting of a single mantle source during the Neogene Siverek phase of the Karacadağ Volcanic Complex, SE Turkey. *Lithos* 146-147: 152-163.
- Ekici T, Macpherson CG, Otlı N, Fontignie D (2014). Foreland magmatism during the Arabia-Eurasia collision: Pliocene-Quaternary activity of the Karacadağ Volcanic Complex, SW Turkey. *Journal of Petrology* 55: 1753-1777.
- Ercan T, Fujitani T, Matsuda JI, Notsu K, Tokel S et al. (1990). Doğu ve Güneydoğu Anadolu Neojen-Kuvaterner Volkanitlerine ilişkin yeni jeokimyasal, radyometrik ve izotopik verilerin yorumu. *MTA Dergisi* 110: 143-164 (in Turkish).

- Fleck RJ, Sutter JF, Elliot DH (1977). Interpretation of discordant  $^{40}\text{Ar}/^{39}\text{Ar}$  age-spectra of Mesozoic tholeiites from Antarctica. *Geochimica et Cosmochimica Acta* 41: 15-32.
- Garcia S, Arnaud NO, Angelier J, Bergerat F, Homberg C (2003). Rift jump process and new paleorift location in northern Iceland for the last 10 Ma based on  $^{40}\text{Ar}/^{39}\text{Ar}$  geochronology. *Earth Planetary Sciences Letters* 214: 529-544.
- Gürsoy H, Tatar O, Piper JDA, Koçbulut F, Mesci BL (2009). Paleomagnetic study of Tertiary volcanic domains in Southern Turkey and Neogene anticlockwise rotation of the Arabian Plate. *Tectonophysics* 465: 114-127.
- Haksal A (1981). Petrographie und Geochemie des Schildvulkans Karacadağ. PhD, Hamburg University, Hamburg, Germany (in German).
- Hill KC, Lucas K, Bradley K (2010). Structural styles in the Papuan Fold Belt, Papua New Guinea: constraints from analogue modelling. In: Goffey PA, Craig J, Needham T, Scott R (editors). *Hydrocarbons in Continental Belts*. London, UK: Special Publications of the Geological Society of London, pp. 33-56.
- Hirano N, Takahashi E, Yamamoto J, Abe N, Ingle SP et al. (2006). Volcanism in response to plate flexure. *Science* 313: 1426-1428.
- Ilani S, Harlavan Y, Tarawneh K, Rabba I, Weinberger R et al. (2001). New K-Ar ages of basalts from the Harrat Ash Shaam volcanic field in Jordan: implications for the span and duration of the upper-mantle upwelling beneath the western Arabian plate. *Geology* 29: 171-174.
- Keskin M (2003). Magma generation by slab steepening and breakoff beneath a subduction-accretion complex: an alternative model for collision-related volcanism in Eastern Anatolia, Turkey. *Geophysical Research Letters* 30: 8046.
- Keskin M, Chugaev AV, Lebedev VA, Sharkov EV, Oyan V et al. (2012a). The geochronology and origin of mantle sources for Late Cenozoic intraplate volcanism in the frontal part of the Arabian Plate in the Karacadağ neovolcanic area of Turkey. Part 1. The results of isotope-geochronological studies. *Journal of Volcanology Seismology* 6: 352-360.
- Keskin M, Chugaev AV, Lebedev VA, Sharkov EV, Oyan V et al. (2012b). The geochronology and origin of mantle sources for Late Cenozoic intraplate volcanism in the frontal part of the Arabian Plate in the Karacadağ neovolcanic Area of Turkey. Part 2. The results of geochemical and isotope (Sr-Nd-Pb) studies. *Journal of Volcanology Seismology* 6: 361-382.
- Koçbulut F, Akpınar Z, Tatar O, Piper JDA, Roberts AP (2013). Palaeomagnetic study of the Karacadağ Volcanic Complex, SE Turkey: monitoring Neogene anticlockwise rotation of the Arabian Plate. *Tectonophysics* 608: 1007-1024.
- Krienitz MS, Haase KM, Mezger K, Van Den Bogard P, Thiemann V et al. (2009). Tectonics events, continental intraplate volcanism, and mantle plume activity in northern Arabia: Constraints from geochemistry and Ar-Ar dating of Syrian lavas. *Geochemistry Geophysics Geosystems* 10: Q04008.
- Lustrino M, Keskin M, Mattioli M, Kavak O (2012). Heterogeneous mantle sources feeding the volcanic activity of Mt. Karacadağ (SE Turkey). *Journal of Asian Earth Sciences* 46: 120-139.
- Lustrino M, Keskin M, Mattioli M, Lebedev VA, Chugaev A et al. (2010). Early activity of the largest Cenozoic shield volcano in the circum-Mediterranean area: Mt. Karacadağ, SE Turkey. *European Journal of Mineralogy* 22: 343-362.
- Mackenzie DE, Johnson RW (1998). Pleistocene Volcanoes of the Western Papua New Guinea Highlands: Morphology, Geology, Petrography, and Modal Chemical Analyses. Report 246. Sydney, Australia: Bureau of Mineral Resources, Geology and Geophysics.
- McKenzie D, Bickle MJ (1988). The volume and composition of melt generated extension of the lithosphere, *Journal of Petrology* 29: 625-679.
- Nakamura K (1977). Volcanoes as possible indicators of tectonic stress orientation - Principle and proposal. *Journal of Volcanology and Geothermal Research* 2: 1-16.
- Nelson ST, Montana A (1992). Sieve-textured plagioclase in volcanic rocks produced by rapid decompression. *American Mineralogist* 77: 1242-1249.
- Pearce JA, Bender JF, DeLong SE, Kidd WSF, Low PJ et al. (1990). Genesis of collision volcanism in eastern Anatolia, Turkey. *Journal of Volcanology and Geothermal Research* 44: 184-229.
- Renne PR, Swisher CC, Deino AL, Karner DB, Owens TL et al. (1998). Intercalibration of standards, absolute ages and uncertainties in  $^{40}\text{Ar}/^{39}\text{Ar}$  dating. *Chemical Geology* 145: 117-152.
- Robertson AHF (2000). Mesozoic-Tertiary tectonic-sedimentary evolution of a south Tethyan oceanic basin and its margins in southern Turkey. In: Bozkurt E, Winchester JA, Piper JDA (editors). *Tectonics and Magmatism in Turkey and the Surrounding Area*. London, UK: Geological Society of London Special Publications, pp. 97-138.
- Roddick JC, Cliff RA, Rex DC (1980). The evolution of excess argon in alpine biotites. *Earth and Planetary Science Letters* 48: 185-208.
- Searle MP (1994). Structure of the intraplate eastern Palmyride Fold Belt, Syria. *Geological Society of America Bulletin* 106: 1332-1350.
- Seyitoğlu G, Esat K, Kaypak, B (2017). The neotectonics of southeast Turkey, northern Syria, and Iraq: the internal structure of the southeast Anatolian Wedge and its relationship with recent earthquakes. *Turkish Journal of Earth Sciences* 26: 105-126.
- Shaw JE, Baker JA, Menzies MA, Thirlwall MF, Ibrahim KM (2003). Petrogenesis of the largest intraplate volcanic field on the Arabian Plate (Jordan): a mixed Lithosphere-Asthenosphere source activated by Lithospheric extension. *Journal of Petrology* 44: 1657-1679.
- Sifré D, Gardes E, Massuyeau M, Hashim L, Hier-Majumder S et al. (2014). Electrical conductivity during incipient melting in the oceanic low-velocity zone. *Nature* 509: 81-85.

Şen PA, Temel A, Gourgaud A (2004). Petrogenetic modelling of Quaternary post-collisional volcanism: a case study of central and eastern Anatolia. *Geological Magazine* 141: 81-98.

Şengör AMC, Özeren MS, Keskin M, Sakıncı M, Özbakır AD et al. (2008). Eastern Turkish high plateau as a small Turkish-type orogen: implications for post-collisional crust forming processes in Turkish-type orogens. *Earth Sciences Reviews* 90: 1-48.

Thy P, Leshner CE, Tegner C (2013). Further work on experimental plagioclase equilibria and the Skaergaard liquidus temperature. *American Mineralogist* 98: 1360-1367.

York D (1969). Least square fitting of a straight line with correlated errors. *Earth Planetary Sciences Letters* 5: 320-324.